Chemical Engineering Journal 525 (2025) 169785

Contents lists available at ScienceDirect

Chemical Engineering Journal

journal homepage: www.elsevier.com/locate/cej

Investigation of micro- and mesomixing in a reaction mixing pump

Seyedeh-Saba Ashrafmansouri [a,c], Arvid Kraus [a,b], Sebastian Osterroth [b], Erik von Harbou [a,*]

[a] Laboratory of Reaction and Fluid Process Engineering, University of Kaiserslautern-Landau, Kaiserslautern, Germany
[b] Department of Flow and Material Simulation, Fraunhofer ITWM, Kaiserslautern, Germany
[c] Department of Chemical Engineering, University of Larestan, Lar, Iran

ARTICLE INFO

Keywords:
Reaction mixing pump
Mixing-sensitive reactions
Villermaux–Dushman reaction
Engulfment model
Micromixing
Backmixing
Process intensification

ABSTRACT

The present study investigates the application of a reaction mixing pump (RMP) as a reactor for mixing-sensitive reactions. In a RMP, the effect of impeller speed and feed rate ratios on the selectivity of the Villermaux–Dushman (VD) reaction system was investigated through experimental means. The observations revealed three distinct mixing regimes, namely backmixing, micromixing and mesomixing, which were dependent on the feed ratio. Increasing impeller speed led to an increase in the selectivity of desired products in the micro- and mesomixing regimes, while it had the opposite effect in the backmixing regime. In the backmixing and mesomixing regimes, selectivity was sensitive to alterations in feed ratio; conversely, in the micromixing regime, changes in feed ratio did not affect the selectivity significantly. In addition, the engulfment micromixing model was utilized to predict selectivities in the micromixing regime, demonstrating a strong correlation with the experimental data. For the first time, the W–Z-transformation was applied to the VD reaction system within the context of the engulfment model. High energy dissipation rates resulted in a reduction of the mixing times to the order of magnitude of 10^{-3} s. This was accompanied by an increase in the selectivity of desired products in the micromixing regime. These observations emphasize the efficiency of RMPs as a promising class of reactors for reactions that are sensitive to mixing.

1. Introduction

Many synthesis are often accompanied by side reactions in which unwanted side-products are formed. The formation of side-products is an inefficient use of raw materials and it reduces the yield of the target product. Furthermore, in many cases it necessitates separation processes downstream of the reactor to obtain the target product with high purity. Achieving higher selectivities to target products in such syntheses is an economically and environmentally important goal. This goal can be achieved not only by chemical means, such as the use of catalysis, but also by physical means, such as the manipulation of mixing intensity, reactor type, and the rate and location of the feed of reactants [1].

The present study focuses on the process of reactant mixing and its influence on the rate of reaction and the product distribution. According to Bałdyga et al. [2], the mixing of chemicals in reactors can be categorized into three distinct scales: macromixing, mesomixing, and micromixing. Macromixing is defined as the homogenization of concentration gradients of the reacting species at the scale of the equipment (the reactor) [3]. In contrast, micromixing can be regarded as the process of mixing of different species at the molecular level [4–7]. The process of mesomixing occurs between these two scales in the region near the feed point of reactants where a plume of fresh feed can be formed [2,6]. Given that reactions between different species occur at the molecular level and that the reactants must be fed into the reactor, in principle, it is necessary to take micro- and mesomixing into consideration in each study of reactions in a given reactor. Nevertheless, for a considerable number of syntheses, the time constant of the reaction rates is found to be higher than the time constant of the micromixing and mesomixing processes. Therefore, these syntheses are solely influenced by macromixing. This means that the mixture is homogenized at the molecular level, and the macroscopic observable concentration profiles of the reacting species within the reactor influence the rates of reactions. This class of reaction systems is frequently designated as “kinetically controlled reactions” [1]. In this work, however, we address another class of reaction systems: the “mixing-sensitive” or “mixing-controlled reactions” [1]. This class of reaction systems is found when the time constant of a reaction is in the same order of magnitude as or less than the time constant for mixing the reactants at the meso and micro scale. While the majority of syntheses are classified

* Corresponding author at: Laboratory of Reaction and Fluid Process Engineering, University of Kaiserslautern-Landau, Kaiserslautern, Germany.
E-mail address: lrf-pub@mv.rptu.de (E.v. Harbou).

https://doi.org/10.1016/j.cej.2025.169785
Received 28 July 2025; Received in revised form 1 October 2025; Accepted 16 October 2025
Available online 21 October 2025

as belonging to the first category, numerous industrially significant reaction systems exhibit a high degree of sensitivity to mixing [1,8,9]. If a given synthesis is sensitive to mixing, both the reactor design and the process conditions (e.g. feed rates) must be carefully chosen to ensure rapid mixing of the reactants after entering the reactor at the feed point and thus to achieve high selectivity to the target products.

In the past, many different reactor types have been proposed for mixing-sensitive reactions. A detailed review on reactors for mixing-sensitive reactions can be found in [10]. In principle, two different categories of mixers (reactors) are used: static and active mixers. Examples, for static mixer designs that are suitable for mixing sensitive reactions are Kenics [11,12], SMV/SMX [12–14], and T- or V-shaped static mixers [15,16]. The stirred tank equipped with an impeller is an example of a reactor that applies active mixing [17,18]. Another example for an active mixer is the rotor–stator spinning disk reactor (rs-SDR) presented by Manzano Martínez et al. [6]. This reactor features a rotating disk encased within a stationary cylindrical housing, creating a high-shear environment that generates intense turbulence and, consequently, effective mixing of the reactants. They observed short mixing times and high selectivities of desired products in this reactor. Following the conclusions of [6], we hypothesize that Reaction Mixing Pumps (RMPs) are also well suited for mixing-sensitive reaction systems due to their special design, which generates high turbulence within the pump. RMPs are a form of peripheral pumps that work similarly to side channel pumps. They feature an impeller with numerous small vanes machined into both sides of its outer edge. This impeller rotates adjacent to a concentric channel within the casing. The interaction of the liquid with the rotating blades of the impeller and the side channels forces the liquid elements into a spiral-shaped flow trajectory. Consequently, the fluid undergoes numerous circulations between the impeller and the side channel as it moves from the pump inlet to the outlet. Moreover, the unique configuration of the impeller leads to the circulation of fluid along its circumference, thereby inducing high internal recirculation flow rates [19]. Due to their reduced volume in comparison to conventional stirred tank reactors, it is anticipated that RMPs will achieve effective macroscopic mixing. Furthermore, the RMPs exhibit a low pump efficiency, leading to a high volumetric energy dissipation within the reaction mixing pump. This property is particularly advantageous for micromixing behavior. Additionally, RMPs combine mixing and transport of the reaction media and thereby leading to a process intensification. In summary, the reaction mixing pump is a potentially viable reactor type for fast mixing-sensitive reactions.

To demonstrate the applicability of the RMP as a reactor for mixing-sensitive reactions, we investigated the product distribution of the Villermaux–Dushman (VD) reaction system under various conditions in a RMP. This reaction has been utilized in numerous studies in conjunction with a variety of reactors, such as stirred tank reactors [20,21], milli- and microflow reactors [22,23], jet reactors [24,25], and rotor–stator spinning disk reactors [6,26]. Consequently, it serves as a valuable tool for assessing the mixing performance of the RMP in comparison to other reactors. Moreover, a comprehensive kinetic model for this reaction system has been documented in the literature [27], thereby enabling modeling and simulation studies. This reaction is also a suitable test reaction due to its straightforward UV spectrophotometric analysis and cost-effectiveness [28].

In this study, the impeller speed of the RMP and feed rate ratios were systematically varied. In addition to the experimental investigations, the well-established engulfment model proposed by Bałdyga and Bourne [29] was employed to model the micromixing behavior within the reactor. This model was chosen for its simplicity and its widespread recognition in the field, making it particularly suitable for the present application. In this work, the engulfment model was utilized for two primary purposes: first, to predict the influence of process parameters on the product distribution within the micromixing regime, and second, to calculate theoretical mixing times based on the experimental results. The W–Z-transformation was applied to the Villermaux–Dushman reaction system within the framework of the engulfment model for the first time. A comparison of the simulated values with the experimental results indicates that the selectivities in the reaction system are determined exclusively by the micromixing process over a wide range of operating conditions.

2. Theory

2.1. Villermaux–Dushman reaction

The Villermaux–Dushman (VD) reaction is a system of competitive parallel reactions that includes an instantaneous neutralization reaction (Reaction (I)), a fast iodide-iodate reaction (Reaction (II)), and an equilibrium iodine-iodide reaction (Reaction (III)). The third reaction produces triiodide ions, which can be detected using a UV–vis spectrometer at a wavelength of 353 nm [20,21,28,30–33].

$$\underbrace{H^+}_{A} + \underbrace{H_2BO_3^-}_{B} \xrightarrow{k_1} \underbrace{B(OH)_3}_{R} \quad \text{(I)}$$

$$6\,\underbrace{H^+}_{A} + \underbrace{IO_3^-}_{C} + 5\,\underbrace{I^-}_{D} \xrightarrow{k_2} 3\,\underbrace{I_2}_{P} + 3\,H_2O \quad \text{(II)}$$

$$\underbrace{I_2}_{P} + \underbrace{I^-}_{D} \overset{K_{eq}}{\rightleftharpoons} \underbrace{I_3^-}_{Q} \quad \text{(III)}$$

Under ideal mixing conditions, the neutralization reaction immediately consumes all available acid, thereby minimizing the occurrence of iodine-iodide reaction and resulting in negligible levels of triiodide ions. However, in cases of poor mixing, localized concentrations of acid form, allowing the neutralization reaction to partially consume the acid and enabling iodide-iodate reaction to proceed, yielding iodine. Subsequent detection of the iodine is accomplished via UV–vis spectroscopy as triiodide ions, which are formed in Reaction (III). Thus, the concentration of the triiodide ions is a measure of the mixing performance [28]. The kinetic model of the VD reaction system is available in Supplementary Material S.1.

2.2. Engulfment model

The engulfment model proposed by Bałdyga and Bourne [29] is a theoretical micromixing model that describes the influence of the local energy dissipation rate and the kinetic viscosity on micromixing behavior [34]. It operates under the assumption that for Schmidt numbers below 4000, micromixing behavior is primarily governed by the entrainment of fluid into turbulent vortices, a process known as engulfment. This assumption is applicable to the present investigations, which involve aqueous solutions with estimated Schmidt numbers in the range of approximately 100 to 1000.

Based on the underlying assumption that engulfment is the controlling mechanism, the engulfment model describes the growth of a reaction zone as bulk fluid is engulfed into the fresh feed. The growth of this volume is ruled by the engulfment rate E, which is given by Eq. (1) [29]. The concept of the engulfment model is sketched in Fig. 1.

$$E = 0.05776\sqrt{\epsilon/\nu} \quad (1)$$

In Eq. (1), ν is the kinematic viscosity of the fluid and ϵ is the local energy dissipation rate [29]. Considering the effect of self engulfment, the volume fraction $X^{(1)}$ of the reaction zone increases over the life time α and can be calculated by Eq. (2) [35].

$$\frac{dX^{(1)}}{d\alpha} = E X^{(1)}\left(1 - X^{(1)}\right) \quad (2)$$

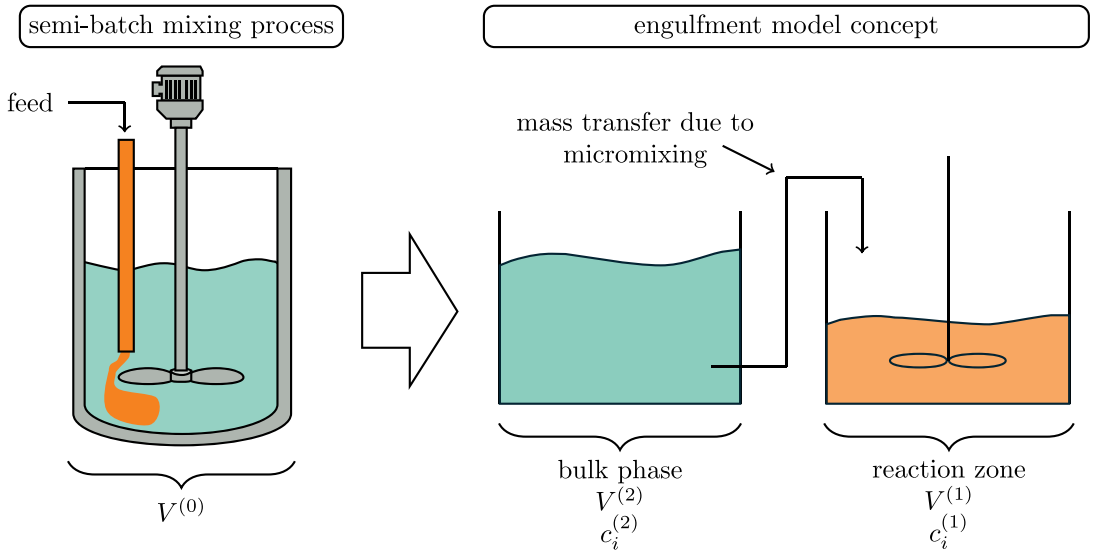

Fig. 1. Concept of the engulfment model. The reactor is divided into a growing reaction zone and a surrounding bulk phase.

The volume fraction of the reaction zone is defined by Eq. (3). Here $V^{(1)}$ represents the increasing volume of the reaction zone and $V^{(0)}$ denotes the total reactor volume.

$$X^{(1)} = \frac{V^{(1)}}{V^{(0)}} \tag{3}$$

Based on Eq. (2), the change of concentration of a substance i in the reaction zone is described by Eq. (4) [35].

$$\frac{\mathrm{d}c_i^{(1)}}{\mathrm{d}\alpha} = E\left(1 - X^{(1)}\right)\left(c_i^{(2)} - c_i^{(1)}\right) + R_i \tag{4}$$

Here, $c_i^{(1)}$ is the concentration of substance i in the growing reaction zone and $c_i^{(2)}$ is the concentration of substance i in the surrounding bulk phase which is engulfed into the reaction zone. R_i is the reaction term of species i inside the reaction zone [29]. Eq. (4) describes the dilution and subsequent reaction of a single fluid element of the acid feed within a surrounding bulk phase.

In this work, the RMP is modeled as an ideal continuous stirred tank reactor (CSTR) based on the assumptions that micromixing is rate-limiting and that macroscopic flow behavior, i.e., large internal circulation flows, causes negligible macroscopic concentration gradients within the RMP. This assumption was confirmed by comparing the residence time behavior of the RMP in tracer experiments with the predictions of the CSTR model in our previous work [36]. To account for micromixing, the dynamic simulation approach proposed by Bourne and Rohani [37] and [35] is adapted, which enables the application of the engulfment model within a CSTR framework. In this approach, the continuous feeds (in this work, acid and buffer flows in the Villermaux–Dushman reaction system) are discretized into finite fluid elements. The volumes of the acid and buffer elements, $\Delta V^{(1)}$ and $\Delta V^{(2)}$, are determined by a macroscopic time step Δt, as described in Eqs. (5) and (6).

$$\Delta V^{(1)} = \Delta t \dot{V}^{(1)} \tag{5}$$

$$\Delta V^{(2)} = \Delta t \dot{V}^{(2)} \tag{6}$$

Here, $\dot{V}^{(1)}$ and $\dot{V}^{(2)}$ denote the flow rates of the acid and buffer streams, respectively, as illustrated in Fig. 2. The fluid elements are introduced sequentially into the reactor, or more precisely, into the bulk phase. First, an acid element k is introduced into the system. For this element, the ODE system resulting from Eqs. (4) and (2) is solved over the interval $\alpha_k = 0$ to $\alpha_{k,\mathrm{end}} = \Delta t$. This approach assumes that all relevant reactions are completed within the duration of the time step, which

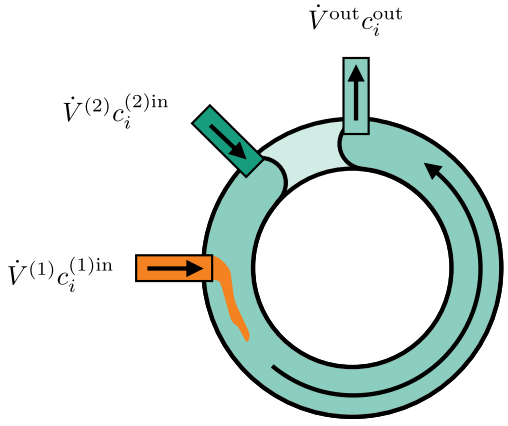

Fig. 2. Flow rates and concentrations in the reaction mixing pump.

imposes a lower limit on the value of Δt. In this case, suitable values for Δt for the combination of the VD system with the RMP range between approximately 0.01 s and 0.1 s. Throughout this calculation, the concentrations of the different species i in the bulk phase are considered constant.

After this, the corresponding buffer fluid element is introduced into the reactor. The concentrations of the fully reacted acid zone, the freshly added buffer, and the remaining bulk phase are then averaged to determine the updated bulk concentrations for the subsequent feed element $k+1$, as described by Eq. (7).

$$c_{i,k+1}^{(2)} = c_{i,k}^{(2)}\left(1 - X_k^{(1)}(\alpha_{k,\mathrm{end}}) - \frac{\Delta V^{(2)}}{V^{(0)}}\right) + c_i^{(2)\mathrm{in}}\frac{\Delta V^{(2)}}{V^{(0)}} + c_{i,k}^{(1)}(\alpha_{k,\mathrm{end}}) X_k^{(1)}(\alpha_{k,\mathrm{end}}) \tag{7}$$

This procedure is repeated iteratively until steady-state concentrations are reached at the reactor outlet. The chemical components of the acid and buffer flows in the VD reaction system are provided in Section 3.

It should be noted that the dynamic simulation approach used in this work is identical to the one proposed by Bourne and Rohani [37]. However, the main difference lies in the formulation of the governing equation: while Bourne and Rohani [37] applied a dimensionless form, this study employs the dimensional form of Eq. (7). The derivation of this equation is provided in Supplementary Material S.8.

The described approach is also applied to estimate micromixing times based on the experimental data. By correlating the engulfment rate E in Eq. (4) with the micromixing time t_{mix} via Eq. (8), an inverse function can be obtained that relates the micromixing time to the experimentally measured selectivities.

$$E = \frac{1}{t_{mix}} \tag{8}$$

It is worth mentioning that the reliability of the calculated micromixing times critically depends on the validity of the underlying modeling assumptions [38].

3. Materials and methods

3.1. Experimental setup

Fig. 3 shows the experimental setup, which comprises the reaction mixing pump (P1). The investigated RMP was a type of peripheral pump comprising a teflon impeller (with a diameter of 0.03 m and a maximum impeller speed of 61 rps), surrounded on both sides by side channels. The RMP is cooled by the transported fluid. Since the pump operates in continuous mode, its temperature is inherently regulated. To provide visual access to the interior of the pump, the original pump head was replaced with a pump head made of poly(methyl methacrylate) (PMMA). The reactor volume, defined as the free space between the inlet and outlet of the pump that can be filled with fluid, was measured to be 1.76 mL. The pump had two inlets for the reactants (buffer flow and acid flow) and one outlet for the products. The buffer solution (an aqueous solution of sodium hydroxide, boric acid, potassium iodate, and potassium iodide) was stored in tank B1. The acid solution (an aqueous solution of perchloric acid) was stored in tank B2. The feed line of the buffer solution was equipped with a valve (V1), a flowmeter (Fl1), and a pressure sensor (PR1). To feed the acid solution into the RMP, a high performance liquid chromatography (HPLC) pump (P2) was employed. The product line was equipped with a thermocouple (TI1) and a pressure sensor (PR2). Both pressure sensors measured the absolute pressure. A needle valve (V2) was installed to regulate the pressure drop in the product line. The product was collected either in a waste tank (B3) or in sample vials, which were used for measuring the concentration of triiodide. The data obtained from the sensors PR1, PR2, and TI1 were recorded by a data logger. A high-speed camera (HSC) and a LED light source was positioned in front of the RMP to record videos. These videos were used to calculate the actual rotational speed of the impeller. The details of the components of the experimental setup are available in Supplementary Material S.2. A figure showing the main dimensions of the RMP is available in Supplementary Material S.3.

3.2. Solution preparation

For each experimental set (group of experiments conducted using the same batch of chemical stock solutions), a 25 L bulk solution was prepared with concentrations as outlined in Table 1. All solutions were prepared using deionized water sparged with nitrogen to remove its dissolved oxygen. This precaution was taken because dissolved oxygen can convert iodide ions to iodine [21]. Additionally, a specific protocol [26,39] was employed to suppress iodine formation during solution preparation. The process began with adding 5 L of boric acid to 5 L of sodium hydroxide solution, resulting in the formation of an equimolar mixture of $H_2BO_3^-$ and $B(OH)_3$ with a pH of 9.14. At this moderately alkaline pH, iodine formation is inhibited [21]. Subsequently, 5 L solutions of potassium iodide and potassium iodate were added to the buffer solution. The total volume was then adjusted to 25 L by adding a 5 L of water. To ensure homogeneity, the buffer solution was mixed thoroughly using a stirrer during preparation. The viscosity and density of the buffer solution at various temperatures, as measured by a Stabinger viscometer, are provided in Supplementary Material S.5. Perchloric acid was diluted with water to achieve the desired concentration, as illustrated in Table 1. In assessing micromixing performance using the VD reaction, sulfuric acid is conventionally utilized. However, this approach has a systematic problem. The second proton available for dissociation of sulfuric acid exhibits lower acidity than the first one, as exemplified by its pK_a values ($pK_{a1} = -3.00$, $pK_{a2} = 1.99$) [40–42]. As such, results obtained using sulfuric acid may not be reliable for short micromixing times. To overcome this limitation, perchloric acid was chosen due to its high strength as a monoprotic acid ($pK_a = -9.24$) [26,27]. pK_a is the negative log of the acid dissociation constant.

Table 1
Concentrations of bulk and acid solutions.

	Compound	Formula	Concentration (mol L^{-1})
Buffer solution	Sodium hydroxide	NaOH	0.0060
	Boric acid	$B(OH)_3$	0.0120
	Potassium iodate	KIO_3	0.0024
	Potassium iodide	KI	0.0120
Acid solution	Perchloric acid	$HClO_4$	0.0500

Considering the potential for oxidation and sensitivity to light, the buffer and perchloric acid solutions were prepared immediately prior to the experiments and used on the same day to prevent degradation. Their exposure to direct light was also avoided [21,26,39]. Details of the suppliers and purities of the chemicals used are listed in Supplementary Material S.4.

3.3. Experimental procedure

3.3.1. Pump characteristic curve

In this work, the flow rate of the RMP (buffer solution) ranged from 4 to 26 L h^{-1}. Initially, the float-type flow meter (FI1) was calibrated using the buffer solution within this range to find a correlation between the float level and the buffer flow rates. Subsequently, the flow rates of 4, 11, 18, and 26 L h^{-1} were selected to determine the pump characteristic curve. For each buffer flow rate, the desired impeller speed of the pump was first selected, and then the needle valve was adjusted to set the flow meter to the desired flow rate based on the calibration curve. After adjusting the buffer flow rate and reaching the steady state (approximately after two minutes), the flow rate was also measured by weighing the vessel of buffer solution before and after a specified period of time. Simultaneously, a video was recorded using the high-speed camera. Finally, the pressures at the inlet and outlet of the RMP, the temperature at the outlet, and the room temperature were recorded at the end of the experiment. The same procedure was applied for all buffer flow rates and impeller speeds to obtain the pump characteristic curve. Each experiment was repeated at least two times, so each data point shown in the subsequent figures represents the mean value of these measurements. These experimental data, along with the uncertainties of our measuring instruments and calculations, are available in Supplementary Material S.13 and S.6.

3.3.2. Reaction experiments

For each experiment involving the reaction, the desired impeller speed of the RMP was first selected, and then the needle valve was adjusted to set the desired buffer flow rate. Next, the acid flow rate was adjusted using the HPLC pump. After adjusting the buffer and acid flow rates and reaching steady state, the vessels containing buffer and acid solutions were weighed before and after a specified period of 2–3 min to determine mass flow rates. Simultaneously, a video was recorded using the high-speed camera. 5 min after the start of the experiment, the inlet pressure, outlet pressure and temperature of the RMP, and room temperature were recorded, and a sample was collected at the outlet of the setup. The sample was analyzed by a UV–vis spectrophotometry

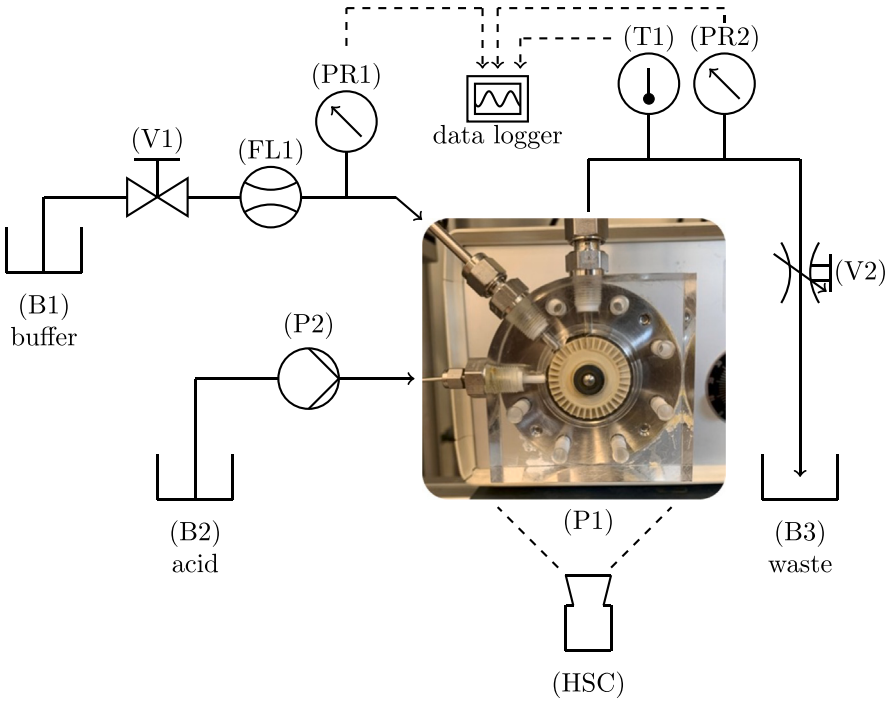

Fig. 3. Experimental setup and reaction mixing pump used in this study.

immediately after collection to measure the concentration of triiodide. The same procedure was used for all flow rates of acid and buffer solutions. More details on UV calibration and sample preparations for UV calibration are available in Supplementary Material S.7. Each experiment was repeated at least twice, so each data point shown in the subsequent figures represents the mean value of these measurements. For experiments with higher flow rates of acid solution (>10 mL min^{-1}), a second HPLC pump (similar to the first one) was connected in parallel to the first HPLC pump to increase the acid flow rate up to 20 mL min^{-1}. All the experimental data, and uncertainties of the measuring instruments and calculations are included in Supplementary Material S.14 and S.6.

3.4. Modeling and calculations

3.4.1. Balance equations

To describe the product distribution of the VD reaction system in the RMP using the engulfment model, Eq. (4) must be solved simultaneously for all species involved in the reaction network. An exception is water, which is produced in the iodine–iodate reaction (Reaction (II)). For water, Eq. (4) does not need to be solved, as its concentration can be assumed constant due to the use of aqueous solutions.

In the kinetic system of the VD reaction proposed by Manzano Martínez et al. [27], the iodine-iodide reaction was characterized by the chemical equilibrium constant K_{eq}, allowing the concentration of triiodide (denoted as Q) to be calculated using an algebraic equation. This approach led to a differential–algebraic equation (DAE) system, where the concentration of triiodide was implicitly tied to the equilibrium condition.

In this work, the modeling approach from Fonte et al. [43] was applied, where the iodine-iodide reaction was modeled as a set of two separate reactions. This modification enabled the entire reaction system to be described by an ordinary differential equation (ODE) system, rather than a DAE system. The reaction rates for the forward reaction ($k_3 = 5.9 \times 10^9$ L mol^{-1} s^{-1}) and for the backward reaction ($k_4 = 7.5 \times 10^6$ s^{-1}) are consistent with the equilibrium constant K_{eq} at 20 °C [44].

In this work, the W–Z-transformation proposed by Bałdyga and Bourne [45] was applied to simplify the solution of the ODE system. Due to the quasi-instantaneous nature of the neutralization reaction, the system is highly stiff, requiring very small time steps and resulting in long computation times. The W–Z-transformation offers an effective way to overcome this issue.

Liu [46] has previously demonstrated the application of the W–Z-transformation to the VD reaction system within the framework of the interaction-by-exchange-with-the-mean (IEM) micromixing model. However, to the best of the authors' knowledge, this transformation has not yet been applied to the VD reaction system in the context of the engulfment model. This work therefore presents such an application for the first time.

The core of the W–Z-transformation is that the first reaction is treated as instantaneous. As a consequence, species A and B cannot coexist in the system at the same time. Consequently, it is necessary to only consider the concentration difference between A and B, as proposed by Burke and Schumann [47]. This approach combines the balance equations in a way that eliminates the reaction term of the first reaction. By doing so, new composition variables, denoted as w and z, are introduced, as defined by Eqs. (9) and (10). This transformation is known as the W–Z-transformation [45].

$$w = c_A - c_B \tag{9}$$

$$z = c_B - c_R \tag{10}$$

Since the reaction rates of the first and second reaction depend on the concentration c_A of hydrogen ions and the concentrations c_B of dihydrogen borate, c_A and c_B must be expressed in terms of the new variable w. Since A and B cannot coexist, the positive part of w corresponds to the concentration c_A (Eq. (11)) whereas the negative part of w corresponds to the concentrations c_B (Eq. (12)).

$$c_A = \frac{|w| + w}{2} \tag{11}$$

$$c_B = \frac{|w| - w}{2} \tag{12}$$

The concentration of boric acid (R) can be calculated according to Eq. (13).

$$c_R = z - \frac{|w| - w}{2} \tag{13}$$

A full description of this procedure is provided in Supplementary Material S.9. For further details, refer to [45]. The resulting balance equations for the reaction zone according to Eq. (4) are given by Eqs. (14) to (19).

$$\frac{dw^{(1)}}{d\alpha} = E\left(w^{(2)} - w^{(1)}\right) - 6k_2\left(\frac{|w^{(1)}| + w^{(1)}}{2}\right)^2 c_C^{(1)} c_D^{(1)2} \tag{14}$$

$$\frac{dc_C^{(1)}}{d\alpha} = E\left(c_C^{(2)} - c_C^{(1)}\right) - k_2\left(\frac{|w^{(1)}| + w^{(1)}}{2}\right)^2 c_C^{(1)} c_D^{(1)2} \tag{15}$$

$$\frac{dc_D^{(1)}}{d\alpha} = E\left(c_D^{(2)} - c_D^{(1)}\right) - 5k_2\left(\frac{|w^{(1)}| + w^{(1)}}{2}\right)^2 c_C^{(1)} c_D^{(1)2} - k_3 c_D^{(1)} c_P^{(1)} + k_4 c_Q^{(1)} \tag{16}$$

$$\frac{dc_P^{(1)}}{d\alpha} = E\left(c_P^{(2)} - c_P^{(1)}\right) + 3k_2\left(\frac{|w^{(1)}| + w^{(1)}}{2}\right)^2 c_C^{(1)} c_D^{(1)2} - k_3 c_D^{(1)} c_P^{(1)} + k_4 c_Q^{(1)} \tag{17}$$

$$\frac{dc_Q^{(1)}}{d\alpha} = E\left(c_Q^{(2)} - c_Q^{(1)}\right) + k_3 c_D^{(1)} c_P^{(1)} - k_4 c_Q^{(1)} \tag{18}$$

$$\frac{dz^{(1)}}{d\alpha} = E\left(z^{(2)} - z^{(1)}\right) \tag{19}$$

3.4.2. Estimation of the energy dissipation rate

According to the model, the engulfment rate is directly correlated with the local energy dissipation rate. In order to compare the experimental observations with the model predictions, the local energy dissipation rate present in the RMP near the acid inlet must therefore be estimated for the chosen operation condition (e.g. the impeller speed). Given the unavailability of simple direct measurements of the local energy dissipation rate, this study employed an estimation approach by calculating the integral energy dissipation rate.

In pump systems, only a portion of the electrical power input is converted into hydraulic power, as a certain amount of the input energy is inevitably dissipated due to mechanical and viscous friction. In the RMP, due to the high Reynolds numbers and the associated high turbulence levels, it is reasonable to assume that the majority of the dissipated power is utilized to generate and sustain turbulence and mixing within the fluid, rather than to overcome mechanical friction. In our experiments, the Reynolds numbers were calculated using Eq. (20) and ranged between 19 800 and 55 350.

$$Re = \frac{N D^2}{\nu} \tag{20}$$

Here, N and D represent impeller speed and impeller diameter, respectively. According to Kolmogorov's turbulence theory [48], energy cascades from large eddies to smaller ones until it is finally dissipated as heat at the smallest scales. This dissipation occurs at the microscale within the fluid, resulting in localized heating that is negligible in terms of its effect on the bulk fluid temperature. Based on this assumption, the energy dissipation rate in the RMP can be estimated using the hydraulic power output and the hydraulic efficiency of the pump, as described in Eq. (21). The derivation of Eq. (21) can be found in Supplementary Material S.10.

$$\epsilon = \left(\frac{1}{\eta} - 1\right)\frac{\Delta p \dot{V}^{(2)}}{\rho V^{(0)}} \tag{21}$$

Here, η, Δp, and ρ are the hydraulic efficiency of the RMP, the static pressure difference between the outlet and inlet of the RMP, and the density of the fluid, respectively. The hydraulic efficiency of the pump describes the ratio of the hydraulic power output of the pump to the mechanical power supplied by the impeller. Based on our previous calculations [36,49], a hydraulic efficiency of 10 % was considered.

3.4.3. The segregation index

The segregation index, often denoted as X_S, is a dimensionless parameter widely used to assess the quality of mixing in fast competitive reaction systems. It quantifies the extent to which an undesired side reaction occurs and serves as a measure of the deviation of a real system from the ideal case of perfect micromixing. The segregation index is defined by Eq. (22), where S_{II} is the selectivity of reactant A toward product Q formed in the side reaction (Reaction (II)), and S_{II}^{ST} represents the corresponding selectivity under the assumption of infinitely slow micromixing [39,50].

$$X_S = \frac{S_{II}}{S_{II}^{ST}} \tag{22}$$

The selectivity S_{II} of the side reaction is determined using Eq. (23), where $\dot{V}^{(1)}$ represents the acid volumetric flow rate and $\dot{V}^{out}$ denotes the total outlet volumetric flow rate ($\dot{V}^{out} = \dot{V}^{(1)} + \dot{V}^{(2)}$). Additionally, $c_A^{(1)in}$ is the inlet concentration of the acid flow, while c_P^{out} and c_P^{out} represent the outlet concentrations of iodine (P) and triiodide (Q).

$$S_{II} = 2\frac{\dot{V}^{out}\left(c_P^{out} + c_Q^{out}\right)}{\dot{V}^{(1)} c_A^{(1)in}} \tag{23}$$

The reference value S_{II}^{ST} corresponds to the theoretical selectivity of the side reaction under the condition of infinitely slow mixing. In such cases, the selectivity depends solely on the inlet concentrations $c_B^{(2)in}$ and $c_C^{(2)in}$ of borate (B) and iodate (C) ions as well as the stoichiometry of the reaction. This reference value can be calculated using Eq. (24) [50]. The derivation of Eq. (24) is provided in Supplementary Material S.11.

$$S_{II}^{ST} = \frac{6c_C^{(2)in}}{6c_C^{(2)in} + c_B^{(2)in}} \tag{24}$$

Since the neutralization reaction occurs almost instantaneously, the selectivity of the side reaction approaches zero under conditions of instantaneous mixing. In contrast, for extremely slow mixing, the selectivity approaches the limiting selectivity. Consequently, the segregation index in this case ranges from 0 to 1, where 0 corresponds to instantaneous mixing and 1 represents infinitely slow mixing. Intermediate values of the segregation index indicate partial mixing, reflecting a state between these two extremes.

In Eqs. (23) and (24), to calculate the segregation index, all the parameters except the concentrations of iodine and triiodide are known. The concentration of triiodide is measured using UV–vis measurements (Supplementary Material S.7), while the concentration of iodine cannot be directly determined. Since iodine participates in an equilibrium reaction forming triiodide, its concentration is linked to the triiodide concentration through a mass balance equation (Eq. (25)):

$$\dot{V}^{out} c_D^{out} = \dot{V}^{(2)} c_D^{(2)in} - \dot{V}^{out}\left(\frac{5}{3}\left(c_P^{out} + c_Q^{out}\right) + c_Q^{out}\right) \tag{25}$$

Using this relation and the equilibrium constant K_{eq} (see Supplementary Material S.1), a second-order polynomial can be derived, where the iodine concentration is the only unknown variable (Eq. (26)).

$$\frac{5}{3}\dot{V}^{out} c_P^{out\,2} + \left(\frac{8}{3}\dot{V}^{out} c_Q^{out} - \dot{V}^{(2)} c_D^{(2)in}\right) c_P^{out} + \frac{\dot{V}^{out} c_Q^{out}}{K_{eq}} = 0 \tag{26}$$

By solving this polynomial equation, the iodine concentration can be determined.

4. Results and discussion

4.1. Pump characteristic curve

Fig. 4 shows the characteristic curve of the reaction mixing pump, which was obtained based on the experimental procedure described in Section 3.3.1. This figure illustrates the pressure difference between the

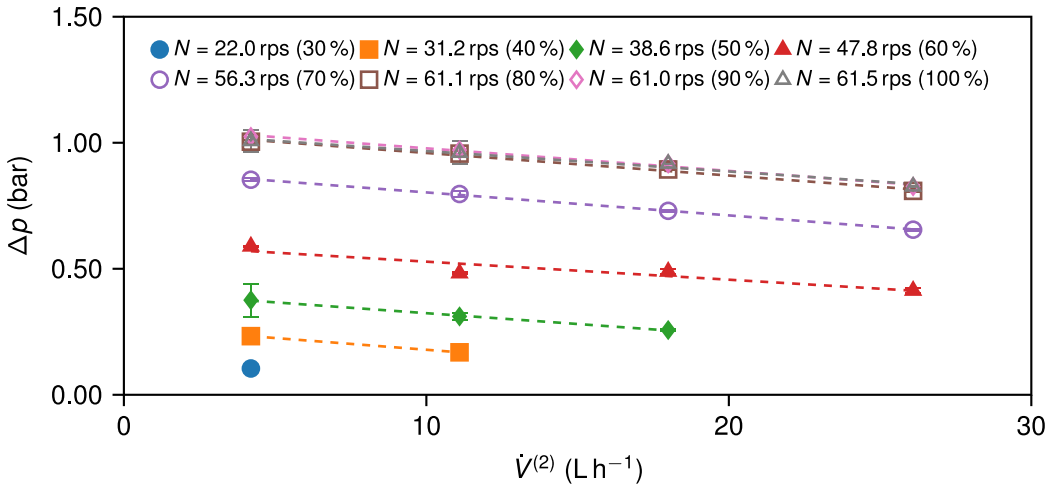

Fig. 4. The characteristic curve of the RMP as a function of the buffer flow rate at different impeller speeds N. The numbers in parentheses are percentages of the maximum impeller speed. Dashed lines were obtained through linear regression and are included as a guide to the eye to illustrate the overall trend.

inlet and outlet of the RMP at different flow rates of the buffer solution and various impeller speeds. As anticipated, an increase in impeller speed results in an increase in pressure difference, under constant volumetric flow rate conditions of the buffer solution. Conversely, at a constant impeller speed, an increase in the buffer flow rate results in a decrease in the pressure difference. As seen in this figure, the changes from 80% to 100% of the maximum impeller speed do not have a significant effect on the pump characteristic curve.

In all figures of the results and discussion section, the experimental data represent the mean values of the measurements, and the error bars indicate the mean absolute errors.

4.2. Reaction experiments

4.2.1. Effect of acid flow rate

Fig. 5 shows the effect of acid feed rate on the segregation index at different impeller speeds. The abscissa represents the acid-to-buffer flow ratio, while the flow rate of the buffer solution is constant ($4\,L\,h^{-1}$), and only the acid flow rate was varied.

Three regimes can be distinguished in Fig. 5. In the regime of a high acid-to-buffer flow ratio (0.10–0.15, indicated by a light blue background color), a decrease in the acid feed rate leads to a decrease in the segregation index. This decrease is observed at all impeller speeds. We hypothesize that the product distribution in this regime is determined by mesomixing, since a decreasing acid flow rate leads to a lower local acid concentration that disperses more quickly. This reasoning is consistent with the conclusions of other researchers [2,6,51–55]. We refer to this regime as the 'mesomixing regime' in the following.

When the acid feed rate decreases further, the segregation index reaches a minimum. This behavior is observed for all impeller speeds, as indicated by the light green background color in Fig. 5. We hypothesize that micromixing determines the product distribution in this regime. To support this, we compared our experimental segregation index results with predictions from micromixing models. A detailed discussion of this issue can be found in Section 4.2.3. Interestingly, decreasing the acid feed rate further increases the segregation index. However, it is generally expected that the feed rate would have no effect in the 'micromixing regime'. This regime is highlighted in light red in Fig. 5. This phenomenon is somewhat similar to the effects observed by Assirelli et al. [56]. They increased the diameter of the feed tube and observed an increase in the segregation index in a semi-batch reactor agitated by a Rushton turbine. Although a different parameter was altered, both a larger capillary diameter and a lower volumetric flow rate result in reduced flow velocity within the feed tube. Under these conditions, it is possible that some of the buffer fluid is pushed back into the acid feed capillary due to centrifugal forces in the RMP. This phenomenon is known as 'backmixing', whereby fluid recirculates into the acid feed capillary. In the backmixing regime, increasing the impeller speed results in a higher segregation index. This observation supports our hypothesis that strong centrifugal forces cause the buffer solution to mix back into the acid feed tube. In contrast, as expected, increasing the impeller speed in the micromixing and mesomixing regimes decreases the segregation index. The segregation index is more sensitive to changes in impeller speed in the mesomixing regime than in the micromixing regime. Fig. 5 also shows that, as the impeller speed increases, the minimum segregation index shifts from left to right.

4.2.2. Backmixing regime

In order to examine the hypothesis that the steep increase of the segregation index for low acid flow rates is indeed caused by backmixing into the feed pipe, additional experiments were conducted at higher acid and buffer flow rates. Fig. 6 shows these experimental data. This figure displays the segregation index as a function of the impeller speed at different volumetric flow rates of acid and buffer solution, while maintaining a constant acid-to-buffer flow rate ratio of 0.014. Based on the observation presented in Fig. 5, this ratio falls within the possible regime of backmixing.

As demonstrated in Fig. 6, an increase in impeller speed is observed to correspond with an increase in the segregation index for all acid and buffer flow rates. As shown in Fig. 6, an increase in impeller speed always results in an increase in the segregation index for all acid and buffer flow rates. This observation supports our hypothesis of backmixing into the feed pipe. Increased impeller speed also leads to greater centrifugal forces being exerted on the fluid in the pump. Centrifugal forces push some fluid element containing the buffer solution into the acid feed pipe, where they react under locally very poor mixing conditions. Consequently, the second and third reactions are more pronounced in this regime, resulting in a higher segregation index on a global scale. It is important to note that the negative impact of higher stirrer speeds on the selectivity is most pronounced at low volumetric flow rates. This phenomenon can be attributed to the observation that a reduced acid volumetric flow rate leads to a decrease in flow velocity within the acid feed pipe. Consequently, there appears to be an increased likelihood of backflow into the feed tube, thereby further substantiating the hypothesis that backflow occurs under these specific conditions. In order to design and scale up RMPs for mixing-sensitive reactions, it is essential to identify and predict the backmixing regime. This will prevent the negative effects of backmixing into the feed pipe on the selectivity.

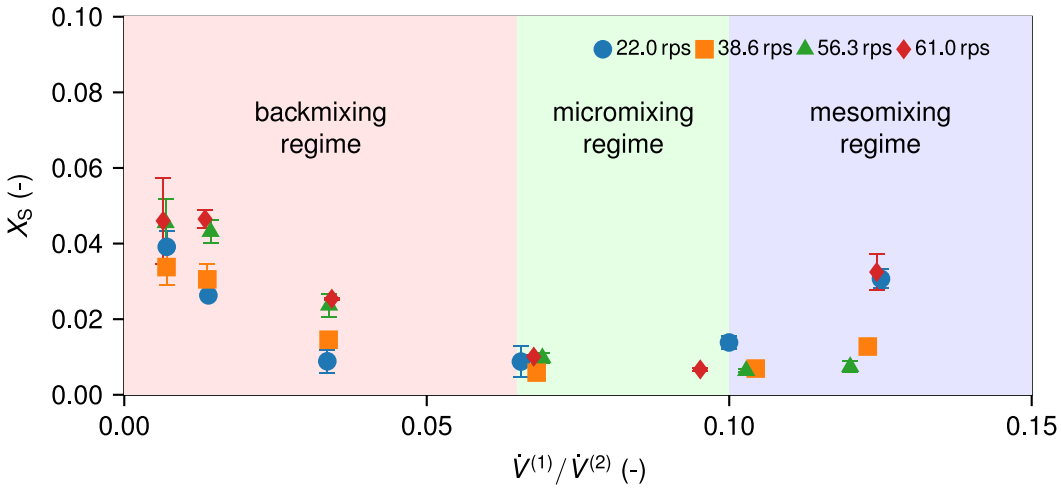

Fig. 5. The effect of acid feed rate on the segregation index at different impeller speeds, and at a constant buffer flow rate of $4\,\mathrm{L\,h^{-1}}$. (For interpretation of the references to color in this figure legend, the reader is referred to the web version of this article.)

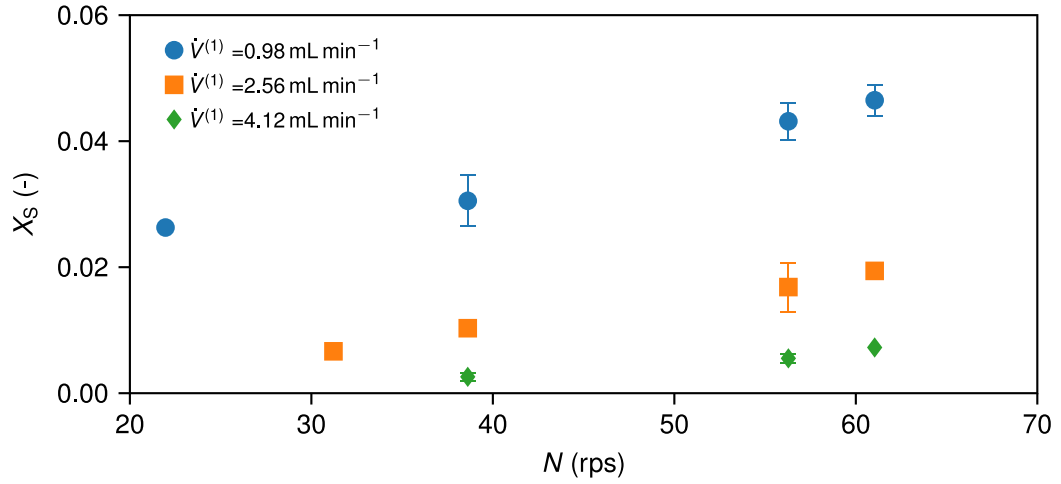

Fig. 6. The segregation index as function of the impeller speed in the backmixing regime at different volumetric flow rates of acid and buffer solutions, while maintaining a constant acid-to-buffer flow rate ratio of 0.014.

4.2.3. Micromixing regime

In order to test the hypothesis that the product distribution is determined by micromixing at medium flow rates of acid feed, additional experiments were performed at a constant acid-to-buffer flow rate ratio of 0.10 (see Fig. 5). In this study, the overall feed rate and impeller speed were both varied. Fig. 7 shows the results of this study. It is evident that increasing impeller speeds, which correspond to higher energy input, results in a decrease of the segregation index to an order of magnitude of 10^{-3}. The segregation index measurements for different overall volumetric flow rates are almost identical within the experimental error. This observation supports the hypothesis of micromixing in this regime, as the reaction selectivity in the case of a micromixing limited process is primarily influenced by the ratio of volumetric flow rates and the local energy dissipation rates. For the lowest feed rate of 7.1 ml/min, a slight increase of the segregation index is observed at the two highest impeller speeds. This finding indicates that the product distribution under these operating conditions is influenced by backmixing due to the relatively low outlet velocity from the feed pipe and the high impeller speed. The segregation index was predicted for the operation conditions of the experiments shown in Fig. 7 using the engulfment model described in Section 2.2. In the figure, model predictions are depicted using hollow markers, while the lines are included solely as guide to the eye. It is important to note that the engulfment model is used to predict the segregation index only at the experimental data points and does not generate a continuous curve. This is because the model relies on the corresponding pressure increase and flow rate values to estimate the energy dissipation rates, which are not available between the measured points. As demonstrated in this figure, there is a strong correlation between the experimental data and the model, thereby validating the hypothesis concerning the presence of a micromixing regime at moderate acid-to-buffer flow rate ratios.

The segregation index, like all selectivities, depends on the specific reaction system. To quantify the mixing behavior purely within the micromixing regime, theoretical mixing times are computed from the experimental data. The necessary correlation between the segregation index and the mixing time is determined using the engulfment model. This correlation is provided in Supplementary Material S.12. Using this correlation, the corresponding mixing time can be determined for each experimental data point. The results are depicted in Fig. 8. The line represents the micromixing time according to Bałdyga and Bourne [29], while the symbols denote our experimental data in the micromixing regime. For comparison, also the experimental data from Manzano Martínez et al. [27] are presented in this figure. They conducted mixing experiments using the VD reaction system in a rotor–stator spinning disk reactor.

As demonstrated in this figure, our experimental findings closely align with the theoretical correlation of the mixing time with the energy

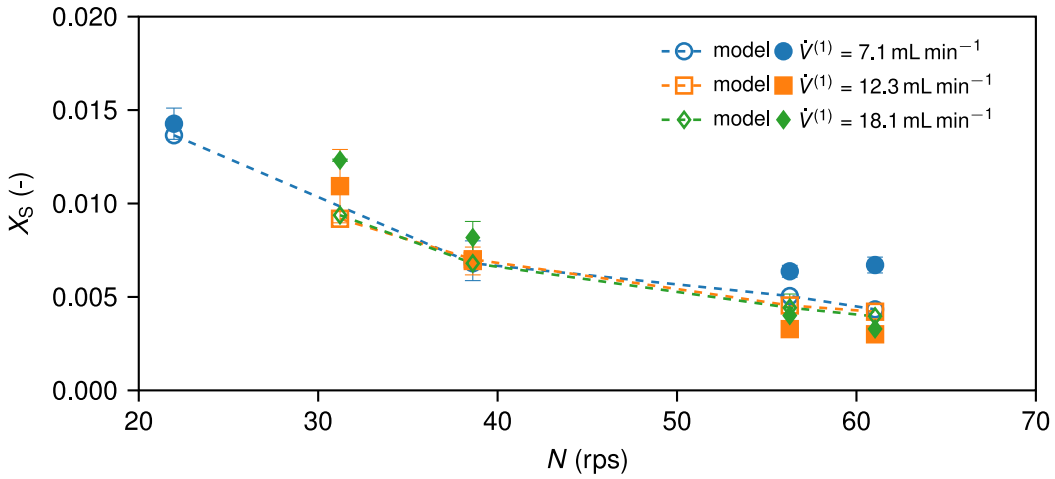

Fig. 7. The segregation index as a function of impeller speed in the micromixing regime at different flow rates of acid and buffer solutions, while maintaining a constant acid-to-buffer flow rate ratio of 0.10.

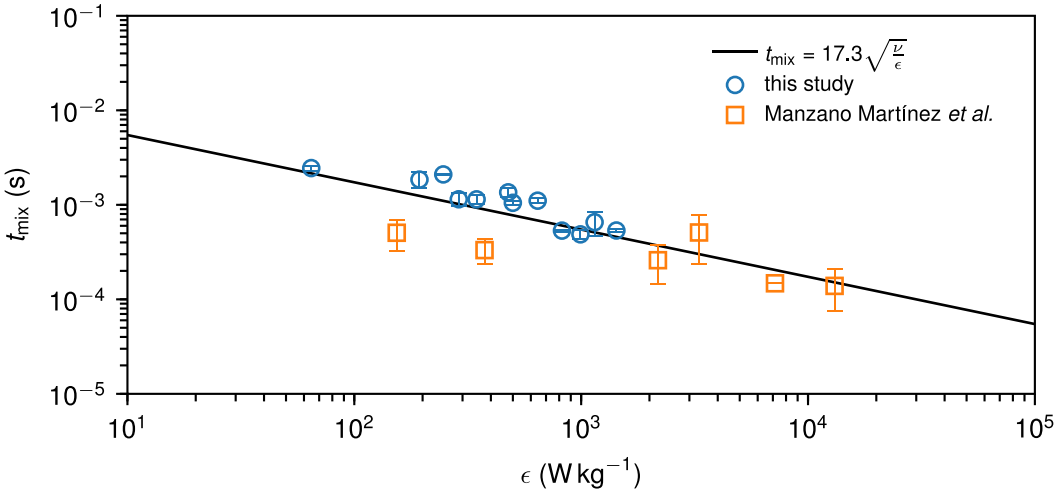

Fig. 8. Mixing times as a function energy dissipation rates. Lines: calculated micromixing time according to Bałdyga and Bourne [29]. Symbols: ∘ — our experimental data obtained in micromixing regime, □ — experimental data from Manzano Martínez et al. [27] (The data including the error bars were extracted by a web-based software [57]).

dissipation rate. This finding confirms our hypothesis, as outlined in Section 4.2.1, that the mixing process in this regime is limited by micromixing. Furthermore, the ranges of energy dissipation rates and mixing times reported in the present work are comparable to the results reported by Manzano Martínez et al. [27]. The discrepancies observed between our findings and those reported by Manzano Martínez et al. [27] can be attributed to the utilization of varying acid concentrations in the respective experiments. In our work, the inlet concentration of acid was 0.05 mol L^{-1}, whereas in [27] it was 0.1 mol L^{-1}.

In addition to Fig. 8, Table 2 also shows a comparison of the performance of different reactors for the VD reaction system. The table shows the order of magnitude of the energy dissipation rate and the order of magnitude of the calculated mixing time based on different micromixing models. Although different acids, acid concentrations, and micromixing models have been used in these studies, the table can provide a rough estimation for comparing different reactors. Although the maximum flow rate of buffer solution in our RMP can be 50 L h^{-1}, the current results are for lower flow rates to reduce the consumption of buffer solution. Consequently, in our RMP, it is anticipated that reduced mixing times can be attained by increasing the flow rate and, consequently, the energy dissipation rates.

5. Conclusion and outlook

In this research, the behavior of a RMP as a reactor for mixing-sensitive reactions was investigated. It was experimentally examined how impeller speed (22–61.5 rps) and feed rate ratios (0.007–0.15) influence the selectivity of the Villermaux–Dushman reaction system in a RMP. At constant impeller speed, three distinct mixing regimes — backmixing, micromixing and mesomixing regime — were observed at low, medium, and high feed rate ratios, respectively. At a constant feed rate ratio, an increase in impeller speed was found to increase selectivity for desired products in the micro- and mesomixing regimes, while it increased selectivity in the backmixing regime. In both the backmixing and mesomixing conditions, selectivity was notably affected by variations in the feed ratio. In contrast, in the micromixing regime, these changes had an insignificant impact on the selectivity.

Furthermore, the engulfment micromixing model was utilized to predict selectivities in the micromixing regime, showing good agreement with our experimental results. In order to enhance the numerical stability of the solver, the W–Z-transformation was utilized. To the best of our knowledge, this is the first application of the W–Z-transformation for the Villermaux–Dushman reaction system within the context of the engulfment model.

Table 2
Comparison of different reactors.

Research	Reactor type	Energy dissipation rate (W/kg)	Mixing time (s)	Micromixing model
Guichardon and Falk [21]	Stirred vessel	10^{-2}-1	10^{-2}-10^{-1}	Incorporation model
Fang and Lee [11]	Kenics static mixer	10^{-2}-1	10^{-3}-10^{-1}	Incorporation model
Manzano Martínez et al. [27]	Rotor–stator spinning-disk reactor	10^{2}-10^{4}	10^{-4}-10^{-3}	Engulfment model
Falk and Commenge [58]	Micromixers	10^{1}-10^{5}	10^{-5}-10^{-3}	IEM model
This work	Reaction mixing pump	10^{1}-10^{3}	10^{-2}-10^{-3}	Engulfment model

High energy dissipation rates (on the order of magnitude of 10^{3} W/kg) led to short mixing times (on the order of magnitude of 10^{-3} s) and high selectivity for desired products (segregation indices on the order of magnitude of 10^{-3}) within the micromixing regime. Given the prevalence of side channel machines in the industry and their demonstrated reliability, it can be assumed that RMPs are generally well accepted in the industry. This innovation could enable process intensification by employing RMPs for both the transport of reaction media and the role of reactors. To extensively utilize this type of reactor, further studies are required to better identify the mixing regimes and their boundaries, so as to control the process conditions to prevent backmixing and increase the potential to work within the micromixing regime.

CRediT authorship contribution statement

Seyedeh-Saba Ashrafmansouri: Writing – review & editing, Writing – original draft, Visualization, Validation, Project administration, Investigation, Data curation, Conceptualization. **Arvid Kraus:** Writing – review & editing, Writing – original draft, Visualization, Validation, Software, Methodology, Formal analysis, Data curation, Conceptualization. **Sebastian Osterroth:** Writing – review & editing, Validation, Methodology, Formal analysis. **Erik von Harbou:** Writing – review & editing, Supervision, Resources, Funding acquisition.

Declaration of competing interest

The authors declare that they have no known competing financial interests or personal relationships that could have appeared to influence the work reported in this paper.

Acknowledgments

The authors would like to express their gratitude to the KSB Foundation for its financial support (No. 1.1377.2022.3). The authors acknowledge the financial support from the High Performance Center for Simulation and Software Based Innovation through a PhD scholarship.

Appendix A. Supplementary data

Supplementary material related to this article can be found online at https://doi.org/10.1016/j.cej.2025.169785.

Data availability

Data will be made available on request.

References

[1] J.R. Bourne, Mixing and the selectivity of chemical reactions, Org. Process. Res. Dev. 7 (2003) 471–508, http://dx.doi.org/10.1021/op020074q.
[2] J. Bałdyga, J.R. Bourne, Y. Yang, Influence of feed pipe diameter on mesomixing in stirred tank reactors, Chem. Eng. Sci. 48 (1993) 3383–3390, http://dx.doi.org/10.1016/0009-2509(93)80155-J.
[3] J. Bałdyga, J.R. Bourne, A fluid mechanical approach to turbulent mixing and chemical reaction part II: Micromixing in the light of turbulence theory, Chem. Eng. Commun. 28 (1984) 243–258, http://dx.doi.org/10.1080/00986448408940136.
[4] Z.-S. Mao, C. Yang, Micro-mixing in chemical reactors: A perspective, Chin. J. Chem. Eng. 25 (2017) 381–390, http://dx.doi.org/10.1016/j.cjche.2016.09.012.
[5] I.S. Ertesvåg, B.F. Magnussen, The eddy dissipation turbulence energy cascade model, Combust. Sci. Technol. 159 (2000) 213–235, http://dx.doi.org/10.1080/00102200008935784.
[6] A.N. Manzano Martínez, R. Jansen, K. Walker, M. Assirelli, J. van der Schaaf, Experimental and modeling study on meso- and micromixing in the rotor–stator spinning disk reactor, Chem. Eng. Res. Des. 173 (2021) 279–288, http://dx.doi.org/10.1016/j.cherd.2021.07.012.
[7] R. David, J. Villermaux, Interpretation of micromixing effects on fast consecutive-competing reactions in semi-batch stirred tanks by a simple interaction model, Chem. Eng. Commun. 54 (1987) 333–352, http://dx.doi.org/10.1080/00986448708911913.
[8] S. Huang, Z. Cui, R. Zhu, C. Chen, S. Song, J. Song, M. Wang, T. Tan, Design and development of a new static mixing bioreactor for enzymatic bioprocess: Application in biodiesel production, Renew. Energy 197 (2022) 922–931, http://dx.doi.org/10.1016/j.renene.2022.08.003.
[9] G.S. Reddy, N.S. Reddy, K. Manudhane, M.V. Rama Krishna, K.J.S. Ramachandra, S. Gangula, Application of continuous flow micromixing reactor technology for synthesis of benzimidazole drugs, Org. Process. Res. Dev. 17 (2013) 1272–1276, http://dx.doi.org/10.1021/op300325f.
[10] J. Bałdyga, J.R. Bourne, Turbulent Mixing and Chemical Reactions, Wiley, New York, 1999.
[11] J. Fang, D. Lee, Micromixing efficiency in static mixer, Chem. Eng. Sci. 56 (2001) 3797–3802, http://dx.doi.org/10.1016/S0009-2509(01)00098-7.
[12] H.E. Meijer, M.K. Singh, P.D. Anderson, On the performance of static mixers: A quantitative comparison, Prog. Polym. Sci. 37 (2012) 1333–1349, http://dx.doi.org/10.1016/j.progpolymsci.2011.12.004.
[13] J.R. Bourne, H. Maire, Micromixing and fast chemical reactions in static mixers, Chem. Eng. Process. Process. Intensif. 30 (1991) 23–30, http://dx.doi.org/10.1016/0255-2701(91)80005-A.
[14] J.R. Bourne, J. Lenzner, S. Petrozzi, Micromixing in static mixers: An experimental study, Ind. Eng. Chem. Res. 31 (1992) 1216–1222, http://dx.doi.org/10.1021/ie00004a037.
[15] M. Engler, N. Kockmann, T. Kiefer, P. Woias, Numerical and experimental investigations on liquid mixing in static micromixers, Chem. Eng. J. 101 (2004) 315–322, http://dx.doi.org/10.1016/j.cej.2003.10.017.
[16] S. Asano, S. Kudo, J.-i. Hayashi, Chaotic-flow-driven mixing in T- and V-shaped micromixers, Chem. Eng. J. 489 (2024) 151183, http://dx.doi.org/10.1016/j.cej.2024.151183.
[17] V. Hessel, H. Löwe, F. Schönfeld, Micromixers: A review on passive and active mixing principles, Chem. Eng. Sci. 60 (2005) 2479–2501, http://dx.doi.org/10.1016/j.ces.2004.11.033.
[18] M. Bayareh, M.N. Ashani, A. Usefian, Active and passive micromixers: A comprehensive review, Chem. Eng. Process. Process. Intensif. 147 (2020) 107771, http://dx.doi.org/10.1016/j.cep.2019.107771.
[19] J.F. Gülich, Kreiselpumpen, Springer Berlin Heidelberg, Berlin, Heidelberg, 2010, http://dx.doi.org/10.1007/978-3-642-05479-2.
[20] J.-M. Commenge, L. Falk, Villermaux–Dushman protocol for experimental characterization of micromixers, Chem. Eng. Process. Process. Intensif. 50 (2011) 979–990, http://dx.doi.org/10.1016/j.cep.2011.06.006.
[21] P. Guichardon, L. Falk, Characterisation of micromixing efficiency by the iodide–iodate reaction system part I: Experimental procedure, Chem. Eng. Sci. 55 (2000) 4233–4243, http://dx.doi.org/10.1016/S0009-2509(00)00068-3.
[22] S.R.L. Gobert, S. Kuhn, L. Braeken, L.C.J. Thomassen, Characterization of milli- and microflow reactors: Mixing efficiency and residence time distribution, Org. Process. Res. Dev. 21 (2017) 531–542, http://dx.doi.org/10.1021/acs.oprd.6b00359.
[23] K. Cheng, C. Liu, T. Guo, L. Wen, CFD and experimental investigations on the micromixing performance of single countercurrent-flow microchannel reactor, Chin. J. Chem. Eng. 27 (2019) 1079–1088, http://dx.doi.org/10.1016/j.cjche.2018.11.026.
[24] W. Pei, X. Li, W. Li, R. Chi, B. Long, J. Guo, J. Zhang, Influence of micromixing and shear on precipitation process in the jet-flow high shear reactors, Chem. Eng. Sci. 300 (2024) 120640, http://dx.doi.org/10.1016/j.ces.2024.120640.
[25] L. Chen, Q. Du, Y. Guo, X. Yang, B. Chen, Numerical modelling of effects of ultrasound-induced acoustic streaming on hydrodynamics in a confined impinging jet reactor using a non-linear model based on local velocity fluctuation, Chem. Eng. Process. Process. Intensif. 183 (2023) 109253, http://dx.doi.org/10.1016/j.cep.2022.109253.

[26] A.N. Manzano Martínez, K.M.P. van Eeten, J.C. Schouten, J. van der Schaaf, Micromixing in a rotor-stator spinning disc reactor, Ind. Eng. Chem. Res. 56 (2017) 13454–13460, http://dx.doi.org/10.1021/acs.iecr.7b01324.
[27] A.N. Manzano Martínez, A.S. Haase, M. Assirelli, J. van der Schaaf, Alternative kinetic model of the iodide–iodate reaction for its use in micromixing investigations, Ind. Eng. Chem. Res. 59 (2020) 21359–21370, http://dx.doi.org/10.1021/acs.iecr.0c04901.
[28] J.M. Reckamp, A. Bindels, S. Duffield, Y.C. Liu, E. Bradford, E. Ricci, F. Susanne, A. Rutter, Mixing performance evaluation for commercially available micromixers using Villermaux–Dushman reaction scheme with the interaction by exchange with the mean model, Org. Process. Res. Dev. 21 (2017) 816–820, http://dx.doi.org/10.1021/acs.oprd.6b00332.
[29] J. Bałdyga, J.R. Bourne, Simplification of micromixing calculations: I. Derivation and application of new model, Chem. Eng. J. 42 (1989) 83–92, http://dx.doi.org/10.1016/0300-9467(89)85002-6.
[30] S.-H. Jung, J.-W. Yeon, Y. Kang, K. Song, Determination of triiodide ion concentration using UV-visible spectrophotometry, Asian J. Chem. 26 (2014) 4084–4086, http://dx.doi.org/10.14233/ajchem.2014.17720.
[31] M.-C. Fournier, L. Falk, J. Villermaux, A new parallel competing reaction system for assessing micromixing efficiency: Experimental approach, Chem. Eng. Sci. 51 (1996) 5053–5064, http://dx.doi.org/10.1016/0009-2509(96)00270-9.
[32] P. Guichardon, L. Falk, J. Villermaux, Characterisation of micromixing efficiency by the iodide–iodate reaction system part II: Kinetic study, Chem. Eng. Sci. 55 (2000) 4245–4253, http://dx.doi.org/10.1016/S0009-2509(00)00069-5.
[33] O.E. Myers, Kinetics of the triiodide equilibrium, J. Chem. Phys. 28 (1958) 1027–1029, http://dx.doi.org/10.1063/1.1744338.
[34] J. Cheng, X. Feng, D. Cheng, C. Yang, Retrospect and perspective of micromixing studies in stirred tanks, Chin. J. Chem. Eng. 20 (2012) 178–190, http://dx.doi.org/10.1016/S1004-9541(12)60378-4.
[35] J. Bałdyga, Simplification of micromixing calculations: II. New applications, Chem. Eng. J. (1989).
[36] S. Eberweiser, Experimentelle Untersuchung Der Fluiddynamischen Eigenschaften Von Reaktionsmischpumpen Zur Beurteilung Ihrer Betriebsbereiche (Ph.D. thesis), Technische Universität Kaiserslautern, 2022, http://dx.doi.org/10.5281/zenodo.16900055.
[37] J.R. Bourne, S. Rohani, Mixing and fast chemical reaction VII: Deforming reaction zone model for the CSTR, Chem. Eng. Sci. 38 (1983) 911–915, http://dx.doi.org/10.1016/0009-2509(83)80012-8.
[38] M. Assirelli, E.J.W. Wynn, W. Bujalski, A. Eaglesham, A.W. Nienow, An extension to the incorporation model of micromixing and its use in estimating local specific energy dissipation rates, Ind. Eng. Chem. Res. 47 (2008) 3460–3469, http://dx.doi.org/10.1021/ie070754n.
[39] E. Tunestål, Investigations of Micromixing: In Alfa Laval's ART® Plate Reactors (Ph.D. thesis), Chalmers University of Technology, 2012.
[40] A. Kölbl, S. Schmidt-Lehr, The iodide iodate reaction method: The choice of the acid, Chem. Eng. Sci. 65 (2010) 1897–1901, http://dx.doi.org/10.1016/j.ces.2009.11.032.
[41] C. Baqueiro, N. Ibaseta, P. Guichardon, L. Falk, Influence of reagents choice (buffer, acid and inert salt) on triiodide production in the Villermaux–Dushman method applied to a stirred vessel, Chem. Eng. Res. Des. 136 (2018) 25–31, http://dx.doi.org/10.1016/j.cherd.2018.04.017.
[42] D. Wenzel, M. Assirelli, H. Rossen, M. Lopattschenko, A. Górak, On the reactant concentration and the reaction kinetics in the Villermaux-Dushman protocol, Chem. Eng. Process.: Process. Intensif. 130 (2018) 332–341, http://dx.doi.org/10.1016/j.cep.2018.06.022.
[43] C.P. Fonte, D.F. Fletcher, P. Guichardon, J. Aubin, Simulation of micromixing in a T-mixer under laminar flow conditions, Chem. Eng. Sci. 222 (2020) 115706, http://dx.doi.org/10.1016/j.ces.2020.115706.
[44] A. Kölbl, M. Kraut, K. Schubert, The iodide iodate method to characterize microstructured mixing devices, AIChE J. 54 (2008) 639–645, http://dx.doi.org/10.1002/aic.11408.
[45] J. Bałdyga, J.R. Bourne, A fluid mechanical approach to turbulent mixing and chemical reaction part III: Computational and experimental results for the new micromixing model, Chem. Eng. Commun. 28 (1984) 259–281, http://dx.doi.org/10.1080/00986448408940137.
[46] L. Liu, Fundamental Study of Shear Controllable Synthesis of Fine Particles using Taylor-Couette Flow Reactor (Ph.D. thesis), Univerisity of Nottingham, England, 2021.
[47] S.P. Burke, T.E.W. Schumann, Diffusion flames, Ind. Eng. Chem. 20 (1928) 998–1004, http://dx.doi.org/10.1021/ie50226a005.
[48] A.N. Kolmogorov, The local structure of turbulence in incompressible viscous fluid for very large Reynolds numbers, Proc. R. Soc. Lond. Ser. A Mathematical Phys. Sci. 434 (1991) 9–13, http://dx.doi.org/10.1098/rspa.1991.0075.
[49] Y. Mayer, Fluid Dynamical and Reaction Engineering Characterization of a Reaction Mixing Pump (Ph.D. thesis), Rheinland-Pfälzische Technische Universität, 2023, http://dx.doi.org/10.5281/zenodo.16812974.
[50] M.-C. Fournier, L. Falk, J. Villermaux, A new parallel competing reaction system for assessing micromixing efficiency: Determination of micromixing time by a simple mixing model, Chem. Eng. Sci. 51 (1996) 5187–5192, http://dx.doi.org/10.1016/S0009-2509(96)00340-5.
[51] J. Bałdyga, J.R. Bourne, Interactions between mixing on various scales in stirred tank reactors, Chem. Eng. Sci. 47 (1992) 1839–1848, http://dx.doi.org/10.1016/0009-2509(92)80302-S.
[52] J. Bałdyga, R. Pohorecki, Turbulent micromixing in chemical reactors: A review, Chem. Eng. J. Biochem. Engineering J. 58 (1995) 183–195, http://dx.doi.org/10.1016/0923-0467(95)02982-6.
[53] L. Vicum, S. Ottiger, M. Mazzotti, Ł. Makowski, J. Bałdyga, Multi-scale modeling of a reactive mixing process in a semibatch stirred tank, Chem. Eng. Sci. 59 (2004) 1767–1781, http://dx.doi.org/10.1016/j.ces.2004.01.032.
[54] M. Jasińska, J. Bałdyga, M. Cooke, A. Kowalski, Application of test reactions to study micromixing in the rotor-stator mixer (test reactions for rotor-stator mixer), Appl. Therm. Eng. 57 (2013) 172–179, http://dx.doi.org/10.1016/j.applthermaleng.2012.06.036.
[55] O. Akiti, P.M. Armenante, Experimentally-validated micromixing-based CFD model for fed–batch stirred–tank reactors, AIChE J. 50 (2004) 566–577, http://dx.doi.org/10.1002/aic.10051.
[56] M. Assirelli, S.P. Lee, A.W. Nienow, Further studies of micromixing: Scale-up, baffling and feed pipe backmixing, J. Chem. Eng. Jpn. 44 (2011) 901–907, http://dx.doi.org/10.1252/jcej.11we042.
[57] A. Rohatgi, WebPlotDigitizer, 2025, URL: https://automeris.io.
[58] L. Falk, J.-M. Commenge, Performance comparison of micromixers, Chem. Eng. Sci. 65 (2010) 405–411, http://dx.doi.org/10.1016/j.ces.2009.05.045.